RSC Advances

PAPER

View Article Online
View Journal | View Issue



Cite this: *RSC Adv.*, 2025, **15**, 4553

# Solvent-free synthesis of 1,2-dihydro-1-arylnaphtho[1,2-*e*] [1,3] oxazine-3-ones using a magnetic nickel–zinc ferrite nanocatalyst†

Sreelakshmi Sreekandan,[a] Anjitha Thadathil,[b] Bindu Mavila,[c] Kannan Vellayan*[a] and Pradeepan Periyat *[c]

Received 29th July 2024
Accepted 13th January 2025

DOI: 10.1039/d4ra05486e

rsc.li/rsc-advances

A high quality magnetic nanocatalyst $Ni_{0.5}$ $Zn_{0.5}Fe_2O_4$ (NZF) was synthesized *via* a sol–gel auto combustion method. The structure and morphology of the synthesized $Ni_{0.5}Zn_{0.5}Fe_2O_4$ (NZF) nanocatalyst were examined using various physico-chemical methods. The catalytic performance of the catalyst with varying transition metal composition was investigated for the solvent-free synthesis of 1,2-dihydro-1-arylnaphtho[1,2-*e*] [1,3] oxazine-3-ones, and it was found that the yield of the product was 87%. The NZF nanocatalyst showed excellent catalytic performance for a wide range of substrates with a very low catalyst loading. The super paramagnetic nature of the NZF nanocatalyst enabled the separation of the catalyst from the reaction mixture by magnetic recovery. Recyclability of the NZF nanocatalyst was also investigated, and it was found that the catalyst exhibited a recyclability of three cycles, without any significant loss in its activity.

## 1 Introduction

The new era of chemistry focuses on the use of inexpensive catalysts, with an eco-friendly aspect, which allow aqueous or solvent-free synthesis without affecting the yield and quality of the product.[1] Nanocatalysis has become an important field to achieve such goals. Nanostructured materials have emerged as powerful heterogeneous catalysts for various organic transformations, in terms of selectivity, reactivity, and improved yields of products. The high surface-to-volume ratio of nanoparticles provides a larger number of active sites per unit area.[2] Nano-catalysts combine the advantages of both homogeneous and heterogeneous catalytic systems, exhibiting high catalytic activity (turnover frequency) and selectivity similar to homogeneous catalytic systems while allowing the recycling and separation of the catalyst after completion of the reaction as shown by heterogeneous catalytic systems.[3]

Magnetically recyclable nano-catalysts (MRNCs) have been recognized for their role in organic synthesis.[4] Such catalytic systems reduce the number of reaction steps, lower the cost of the process and minimize waste generation.[5] Recently, multimetallic systems with magnetic properties have been used as catalysts for conducting one-pot multistep reactions.[6] Multimetallic nanoparticles, which contain more than two distinct metals, exhibit synergistic effects that enhance the catalytic activity.[7] These multimetallic nanoparticles combine the properties of their individual constituents, resulting in characteristics that are superior to those of their constituents, thereby achieving improved activity, selectivity and stability.[8] The difference in electronegativity between the individual metal nanoparticles can induce electron transfer, leading to the generation of electron-poor and -rich regions on the multi metallic surface. This electronic effect promotes high electron uptake and increases the electron transfer between the target molecules, resulting in a high catalytic activity of multi metallic nanocatalysts.[9]

According to previous researches, trimetallic NPs exhibit unique characteristics and demonstrate higher reactivity than bimetallic and monometallic nanomaterials. They can be employed as efficient nanocatalysts, antimicrobials and anticancer agents.[10] Trimetallic nanocatalysts display enhanced catalytic performance and higher stability, making them promising photocatalysts and adsorbents for the elimination of hazardous pollutants and contaminants.[11]

Ferrite nanoparticles provide increased surface area for organic groups to anchor, which enhances the product yield and reduces the reaction time, providing a cost-effective and efficient method for organic transformations.[12] Various organic reactions are reported, such as the photocatalytic decomposition of different dyes, alkylation, dehydrogenation, oxidation and C–C coupling, with nano-ferrites as the catalyst.[13] Multimetallic ferrites such as Ni–Mg–Zn ferrite, Ni–Co–Zn ferrite, Ni–

[a]*Department of Chemistry, Government College, Kattappana, Kerala, India. E-mail: kannanpvl@gmail.com*

[b]*Department of Chemistry, University of Calicut, Kerala, India*

[c]*Department of Environmental Studies, Kannur University, Kerala, India. E-mail: pperiyat@kannuruniv.ac.in*

† Electronic supplementary information (ESI) available. See DOI: https://doi.org/10.1039/d4ra05486e

Zn–Al ferrite, Pd–Bi ferrite, Co–Sm ferrite, Co–Ce ferrite, Mg–Ce ferrite, and Co–Zn–Gd ferrite have been proven to be promising materials for waste water treatment, computer memory, electromagnetic interference filtration, transesterification and gas sensing applications.[14–22] The pure zinc ferrite ($ZnFe_2O_4$) and $ZnNd_2O_4$ have demonstrated high activity for the coupling reaction.[23] Ferrite nanomaterials have been employed as a catalyst for condensation and cyclization reactions, oxidation of various alkenes, alkylation, C–C coupling, dehydrogenation reactions and synthesis of organic compounds such as arylamines and acetylferrocene chalcones.[11,24] CuO nanoparticles are potential candidates, showing antibacterial effect against both Gram-negative and Gram-positive bacteria.[25,26] Magnetic nanodendrimers have shown promising catalytic activity for a wide variety of organic transformations such as coupling, reduction, cycloaddition and oxidation.[27] Green-synthesized $Zn_{0.5}Ni_{0.5}FeCrO_4$ magnetic nanoparticles (MNPs), which are magnetically recoverable, exhibit significant photocatalytic activity due to their unique composition, which enhances the generation of reactive species when exposed to light. Their synthesis through environmentally friendly methods often involves the use of plant extracts, which not only reduces the use of harmful chemicals but can also enhance the properties of nanocatalysts.[28]

The recovery of catalysts from the system is a crucial characteristic for the catalyst to be acceptable in green chemical manufacturing processes in industry. The ferrite nanocatalysts can be separated easily from reaction systems using an external magnet and can be reused with minimal loss of catalytic activity. Magnetic separation reduces secondary waste generation and energy consumption.[29] Multicomponent reactions are gaining increasing interest in the synthesis of biologically important compounds, as they simplify the possess of building up complex molecules.[30]

Heterocyclic compounds (HC) with five and six membered rings play a vital role in medicinal chemistry, thus making the synthesis of heterocycles with reusable nanocatalysts increasingly important in the pharmaceutical and organic chemistry fields. Oxazinone, benzoxazinone and their derivatives are important classes of heterocyclic compounds that exhibit biological activities, such as HIV-1 reverse transcriptase inhibitors.[31]

Various heterocyclic compounds have demonstrated antibacterial, antifungal, antiviral and anti-inflammatory properties.[32] Heterocycles constitute a common structural unit of most marketed drugs, with 60% of unique small-molecule drugs containing nitrogen.[33] Recent advancements have utilized nanoparticles as effective catalysts in the synthesis of nitrogen-containing heterocyclic compounds; for example, MgO nanocatalysts have been employed in the preparation of dihydropyrano [2,3-*c*]pyrazole derivatives.[34] Additionally a Schiff base complex of copper immobilized on core–shell magnetic nanoparticles Cu(II)-SB/GPTMS@$SiO_2$@$Fe_3O_4$ has been reported to be efficient in the synthesis of biologically active polyhydroquinoline derivatives.[35,36]

2-Naphthol and naphthoxazinones and their derivatives were reported to possess bactericidal, antioxidant and chelating properties in the metal-catalysed asymmetric synthesis and they have cytotoxic and antifungal activities.[37,38] Chiral Mannich bases of β-naphthol are commonly used as metal-mediated and ligand-accelerated catalysts in enantioselective carbon–carbon bond formation.[39,40]

Various strategies employing harsh reaction conditions have been reported for the synthesis of 1,2-dihydro-1-arylnaphtho [1,2-*e*] [1,3] oxazine-3-ones by the condensation of aldehyde with β-naphthol and urea in the presence of $FeCl_3$ under microwave assistance,[41] thiamine hydrochloride catalyst in alcohol[42] and $Sr(OTf)_2$ as the catalyst in chloroform.[43] It is desirable to develop a more efficient, simple, less expensive and less toxic one-pot method for the synthesis of 1,2-dihydro-1-aryl naphtho[1,2-*e*] [1,3] oxazine-3-ones. In this work, we demonstrate a method to extend the scope of the three-component condensation of β-naphthol, aryl aldehydes and urea, using efficient, readily available, simply synthesized and magnetically retrievable nickel zinc ferrite (NZF) nanoparticles as the catalyst under solvent free conditions.

## 2 Experimental

### 2.1 Synthesis of $Ni_{0.5}Zn_{0.5}Fe_2O_4$ (NZF) nanocatalysts

The nanocatalyst $Ni_{0.5}Zn_{0.5}Fe_2O_4$ (NZF) was synthesized by a sol–gel auto combustion method (Scheme 1).[43–45] Solutions of iron nitrate ($Fe(NO_3)_3 \cdot 9H_2O$) at a concentration of 2.0 M, nickel nitrate ($Ni(NO_3)_2 \cdot 6H_2O$) at a concentration of 0.5 M and zinc nitrate ($Zn(NO_3)_2 \cdot 6H_2O$) at a concentration of 0.5 M were used as the precursors for the nanoparticle synthesis. The iron nitrate, nickel nitrate, and zinc nitrate solutions were mixed

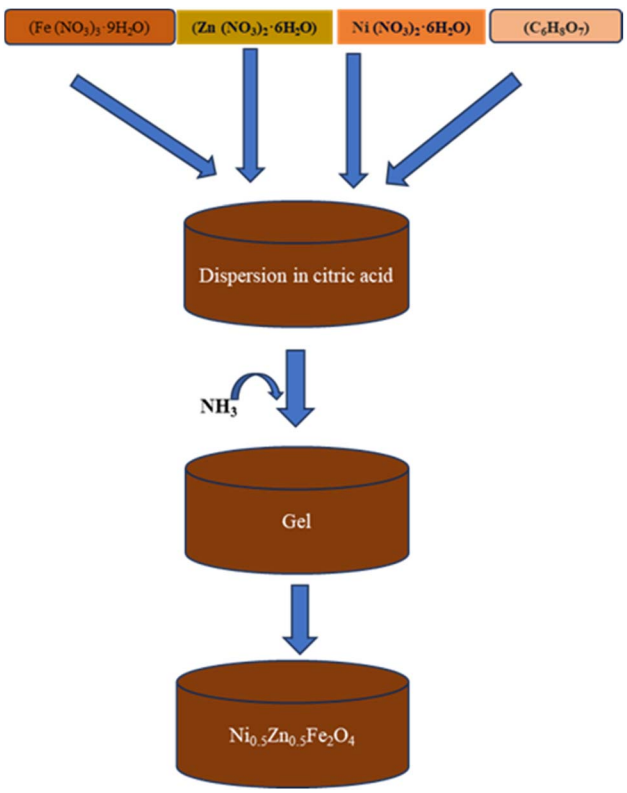


Scheme 1 Synthesis of the $Ni_{0.5}Zn_{0.5}Fe_2O_4$ nanocatalyst.

thoroughly with citric acid ($C_6H_8O_7$) at a concentration of 2.2 M to form a clear solution. The pH of the solution was adjusted to 7 by the addition of ammonia solution. This step was important to create optimal conditions for the gel formation. The solution was stirred continuously and kept at a temperature of 90 °C until a gel-like substance formed. The gelling process helped to form the desired nanoparticle structure. The gel was then heated to 150 °C to initiate a self-propagating combustion process. This combustion helped to further transform the gel into the desired NZF nanoparticle structure. The resultant loose powder from the combustion process was crushed well to break down any large particles. This step ensured uniform particle size distribution. The crushed powder was then calcined at a temperature of 550 °C for 4 h. It helped further solidification of particles and formation of the spinal phase. The ratio of nitrates to citric acid used in the synthesis is 1 : 2.77. This ratio had been optimized to obtain the desired properties of the NZF nanoparticles.

### 2.2 Characterisation of $Ni_{0.5}Zn_{0.5}Fe_2O_4$ (NZF) nanocatalysts

The as synthesized $Ni_{0.5}Zn_{0.5}Fe_2O_4$ (NZF) nanocatalysts were characterized by powder X-ray diffraction (XRD) (X'Pert3 Powder with CuKα ($\lambda$ = 1.5406 Å) radiation) and FTIR spectroscopy (JASCO FTIR-model 4100, in the range of 350–4000 $cm^{-1}$ by the KBr pellet method).

The morphology was investigated by scanning electron microscopy (Hitachi S-3000H) and transmission electron microscopy (JEOL/JEM2100 with a 200 kV accelerating voltage and a lattice resolution of 0.14 nm) analysis.

The XRD pattern of the catalyst shows an average size of 10 nm, calculated using the Scherrer formula in eqn (1). The broadening of diffraction peaks can be attributed to the bulk to nanoscale conversion of crystallite sizes.

$$D = \kappa\lambda/(\beta \cos\theta) \quad (1)$$

The Scherrer formula describes the broadening of a peak at a particular diffraction angle ($\theta$), where $D$ is the crystalline domain size and $\beta$ is the width of the peak at half of its height. The Scherrer constant $\kappa$ is typically considered to be 0.91 but can vary with the morphology of the crystalline domains and $\lambda$ is the wavelength of X-rays used.

These well characterized $Ni_{0.5}Zn_{0.5}Fe_2O_4$ (NZF) nanocatalysts were used for the synthesis of 1,2-dihydro-1-arylnaphtho[1,2-*e*][1,3] oxazine-3-ones.

### 2.3 Synthesis of 1,2-dihydro-1-arylnaphtho [1,2-*e*] [1,3] oxazine-3-ones using $Ni_{0.5}Zn_{0.5}Fe_2O_4$ (NZF)

A mixture of aryl aldehyde (1 mmol), β-naphthol (1 mmol) and urea in the presence of the $Ni_{0.5}Zn_{0.5}Fe_2O_4$ catalyst (80 mg) was stirred under solvent free conditions at a temperature of 120 °C. The progress and completion of the reaction were monitored by thin layer chromatography. The insoluble catalyst was magnetically removed and the solvent was evaporated from the reaction mixture followed by column chromatography over silica gel using the solvent mixture of chloroform-ethyl acetate (7 : 3) to get the pure product. The product was then characterised by $^1$H NMR (nuclear magnetic resonance) spectroscopy to determine the molecular structure.

## 3 Results and discussion

### 3.1 Catalyst characterization

**3.1.1 X-ray diffraction.** The X-ray diffraction technique is a powerful non-destructive method to understand the crystallographic structure, chemical composition and physical properties of nanocatalysts.[46] The XRD patterns of nickel ferrite (NF) and $Ni_{0.5}Zn_{0.5}Fe_2O_4$ (NZF) nanoparticles are shown as Fig. 1. The reflections corresponding to the (111), (220), (311), (222), (400), (331), (422), (511) and (440) lattice planes in the XRD patterns of ferrite nanoparticles confirmed the formation of a spinel cubic structure belonging to the $Fd\bar{3}m$ space group. The characteristic diffraction peaks were in good agreement with JCPDS-00-008-0234. Each peak can be evaluated independently and should produce a consistent crystalline domain size as long as the sample can be roughly approximated as uniform, spherical particles.

The average crystallite size ($D$) of the NZF nanoparticles (10 nm) was calculated from the broadening of the most intense peak (311) of the sample. The crystallite size increases when more $Ni^{2+}$ ions are replaced by $Zn^{2+}$ ions (0.83 Å) with a large size compared to $Ni^{2+}$ ions (0.78 Å).

**3.1.2 FT-IR spectral analysis.** FT-IR spectra of the NZF nanocatalyst are shown as Fig. 2. It has been reported that the distinct IR bands of solids correspond to the vibrational modes and position of ions in the crystal lattice.[47] Notably two main absorption bands have been observed in the fingerprint region around 350–590 $cm^{-1}$. These bands were attributed to the stretching vibration of metal ion-oxygen bonds in the tetrahedral and octahedral sites. For NZF nanoparticles, the octahedral and tetrahedral M–O stretching vibrations have been observed at 396 $cm^{-1}$ and 579 $cm^{-1}$, respectively. The splitting of the absorption bands has been attributed to the local lattice

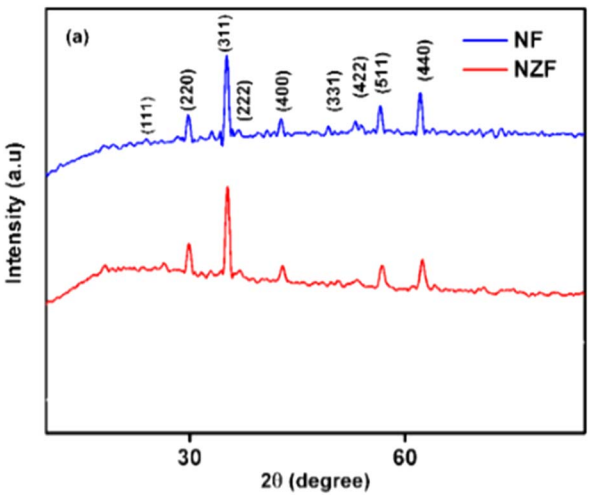


Fig. 1 X-ray diffraction patterns of nickel ferrite (NF) and $Ni_{0.5}Zn_{0.5}Fe_2O_4$ (NZF) nanoparticles.

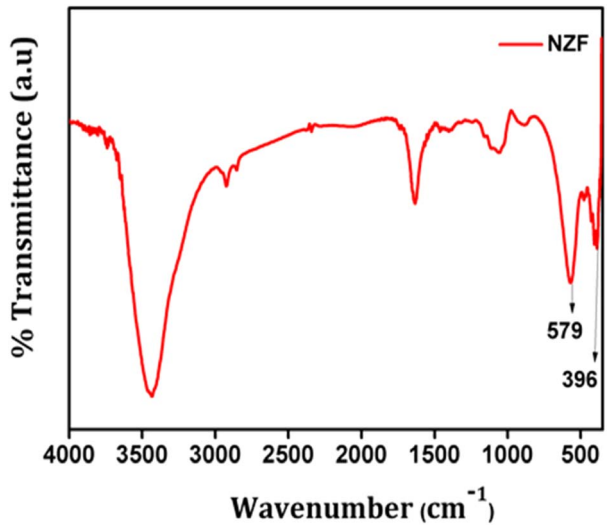


Fig. 2 FTIR spectra of NZF nanoparticles.

deformation, as evident from the spectra.[48,49] Additionally, a peak observed at 3403 $cm^{-1}$ has been attributed to the symmetric stretching vibration of –OH groups of adsorbed water.

**3.1.3 SEM and TEM analysis.** The morphology and size distribution of the NZF nanoparticles have been examined by SEM analysis and it was found that the particles have slight agglomeration as shown in Fig. 3(a). The nanoparticles tend to agglomerate and grow into larger assemblies, which may be attributed to their high surface energies.[50] TEM micrographs of nanocrystalline NZF nanoparticles are shown as Fig. 3(b). In the TEM image, most of the particles exhibited roughly spherical structures. The $Ni_{0.5}Zn_{0.5}Fe_2O_4$ (NZF) nanocatalysts synthesized in the current study have an average particle size of 10 nm.

**3.1.4 Magnetic properties of NZF nanoparticles.** The magnetic properties measured for NZF are listed in Table 1. Ni–Zn ferrites are associated with high magnetic permeability.[51] The total magnetization of the NZF system increased due to the increase of inter-sublattice A–B super exchange interaction between the magnetic ions of A and B sublattices. In nickel zinc ferrites of spinel structure, the tetrahedral A sites have been

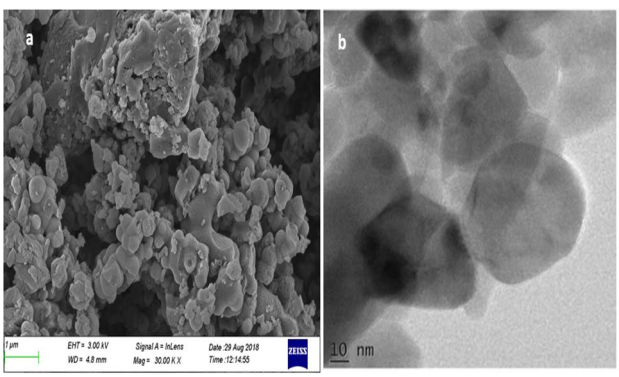


Fig. 3 (a) SEM and (b) TEM images of NZF nanoparticles.

Table 1 Magnetic properties of NZF nanoparticles[a]

| Nanoparticles | $T_B$ (K) | $M_s$ (emu $g^{-1}$) | $M_r$ (emu $g^{-1}$) | $H_c$ (Oe) |
|---|---|---|---|---|
| NZF | 56.2 | 45.38 | 4.85 | 28.8 |

[a] $T_B$ (K): blocking temperature, $M_s$ (emu $g^{-1}$): saturation magnetization, $M_r$ (emu $g^{-1}$): remanent magnetization and $H_c$ (Oe): coercivity.

strongly favoured to be occupied by $Zn^{2+}$ ions and the octahedral B sites by $Ni^{2+}$ ions. The cation distribution in NZF can be expressed by $(Zn_xFe_{1-x})_A$ $(Ni_{1-x}Fe_{1+x})_BO_4$. As nonmagnetic $Zn^{2+}$ ions are introduced to the NF system, it pushes more $Fe^{3+}$ ions from tetrahedral A sites to octahedral B sites, and as a result the magnetic moment of the B site increases. Therefore, the total magnetization increases; this increase in saturation magnetization is in good agreement with Néel's collinear two-sublattice model.[52,53]

### 3.2 Synthesis of 1,2-dihydro-1-arylnaphtho[1,2-*e*] [1,3] oxazine-3-ones

After the synthesis and complete characterisation of the NZF nanocatalyst, the nanocatalyst has been scrutinized in the synthesis of 1,2-dihydro-1-arylnaphtho[1,2-*e*] [1,3] oxazine-3-ones. Various parameters such as reaction conditions, type of solvent used, reaction time, temperature and the amount of catalyst loading have been optimised.

Solvent free condition has been tested at various temperatures starting from 30 °C. The maximum yield has been obtained at 120 °C, and no further increase in yield was obtained when increasing the temperature. In order to study the effect of the catalyst, the reaction has been carried out in the absence of

Table 2 Optimization of solvents in the synthesis of 1,2-dihydro-1-arylnaphtho[1,2-*e*] [1,3] oxazine-3-ones

| Solvent | Time (min) | Yield (%) |
|---|---|---|
| Water | 120 | 45 |
| Ethanol | 120 | 72 |
| Toluene | 120 | 55 |
| DCM | 120 | 65 |
| Solvent free | 120 | 87 |

Table 3 Optimization of catalyst loading for the synthesis of 1,2-dihydro-1-arylnaphtho[1,2-*e*] [1,3] oxazine-3-ones

| Amount of catalyst (g) | Time (min) | Yield (%) |
|---|---|---|
| 0.020 | 120 | 64 |
| 0.030 | 120 | 69 |
| 0.040 | 120 | 71 |
| 0.050 | 120 | 76 |
| 0.060 | 120 | 78 |
| 0.070 | 120 | 82 |
| 0.080 | 120 | 87 |
| 0.090 | 120 | 87 |

Table 4 Comparison of catalytic performance of the NZF nanocatalyst with other multimetallic nanocatalysts in the synthesis of 1,2-dihydro-1-arylnaphtho[1,2-*e*] [1,3] oxazine-3-ones

| Catalyst | Reaction condition | Yield % | Reference |
|---|---|---|---|
| $Co_{0.5}Mg_{0.5}Al_2O_4$ | Solvent-free | 52 | — |
| ZnO | Solvent-free | 74 | 45 |
| $Fe_3O_4$ | Solvent-free | 54 | 46 |
| $Ni_{0.5}Zn_{0.5}Fe_2O_4$ | Solvent-free | 87 | NZF catalyst |

the catalyst under the same reaction condition. A trace amount of product was obtained, clearly indicating the role of the catalyst.

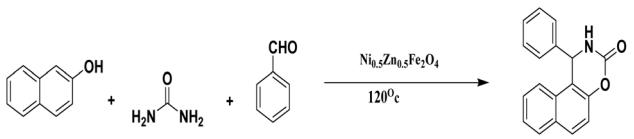


Scheme 2 Synthesis of 1,2-dihydro-1-arylnaphtho[1,2-*e*] [1,3] oxazine-3-ones under optimized conditions.

**3.2.1 Solvent screening studies.** To investigate the effect of solvents on the synthesis of 1,2-dihydro-1-arylnaphtho[1,2-*e*] [1,3] oxazine-3-ones, solvents such as water, ethanol, dichloromethane (DCM) and toluene have been used and the % yield is summarized in Table 2 [the amount of catalyst used was 80 mg and the reactions were carried out at 120 °C]. The catalytic reaction yielded a moderate result in the polar aprotic solvent DCM. The reaction showed little progress in water. Among the solvents selected, ethanol gave a better yield of 72%, whereas under solvent free conditions 87% yield was obtained.

**3.2.2 Effect of catalyst loading.** The amount of catalyst has been varied as 20, 30, 40, 50, 60, 70 and 80 mg and the results are summarized in Table 3. The optimum catalyst loading has been found to be 80 mg, and a further increase in the amount of catalyst did not lead to any change in the yield.

**3.2.3 Effect of temperature.** To optimize the temperature, a mixture of β-naphthol (1 mmol), aldehyde (1 mmol) and urea (1 mmol) has been heated in the presence of 80 mg of NZF nanocatalyst under solvent free conditions, at various temperatures ranging from 30 °C to 150 °C. The maximum yield has been obtained at 120 °C.

A comparison of catalytic activity of $Ni_{0.5}Zn_{0.5}Fe_2O_4$ (NZF) nanocatalysts with that of other catalysts in the solvent free

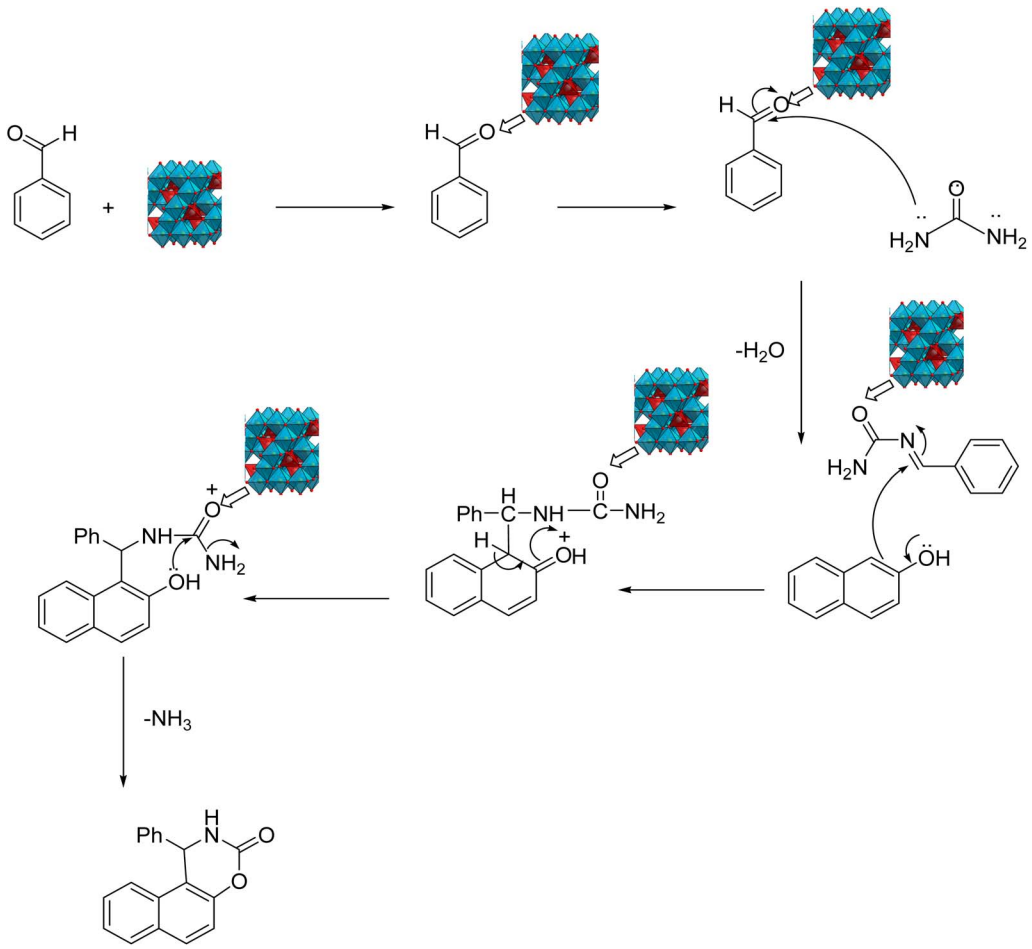


Scheme 3 Proposed mechanism for the synthesis of 1,2-dihydro-1-arylnaphtho[1,2-*e*] [1,3] oxazine-3-ones using NZF nanoparticles.

synthesis of 1,2-dihydro-1-arylnaphtho[1,2-*e*] [1,3] oxazine-3-ones is given in Table 4.

In summary, the optimization studies revealed that the $Ni_{0.5}Zn_{0.5}Fe_2O_4$ (NZF) nanocatalyst showed good yield in the synthesis of 1,2-dihydro-1-arylnaphtho[1,2-*e*] [1,3] oxazine-3-ones with a reaction time of 120 minutes at 120 °C under solvent free conditions (Scheme 2).

The proposed mechanism for the synthesis of 1,2-dihydro-1-arylnaphtho[1,2-*e*] [1,3] oxazine-3-ones is shown as Scheme 3. In the initial step, reactants get adsorbed on the surface of the catalyst. The nanocatalyst bears high surface area, which increases the adsorption of reactant molecules. The unique surface chemistry associated with the nanocatalyst and higher zeta potential value help in the stabilization of the nanocrystal system.[54,55] In NZF, $Zn^{2+}$ is the main active component having Lewis acid properties and superior catalytic properties.[56,57] The NZF catalyst activates the carbonyl group of the aldehyde *via* co-ordination of the vacant orbital present on $Ni^{2+}$ with carbonyl oxygen. The carbonyl group is then polarized because of the difference in electronegativities between carbon and oxygen. After this step, the unshared pair of electrons in the nitrogen atom of amine is attracted to the partially positive carbon of the

Table 5 Synthesis of 1,2-dihydro-1-arylnaphtho[1,2-*e*] [1,3] oxazine-3-ones by varying the aldehydes[a]

| Sl. no. | β-Naphthol | Aldehyde | Urea | Product | Yield % | M.P. (°C) |
|---|---|---|---|---|---|---|
| 1 | 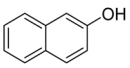 |  | 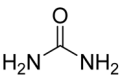 | 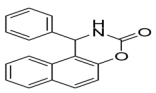 | 87 | 216 |
| 2 | 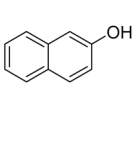 | 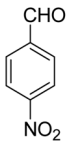 | 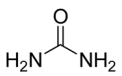 | 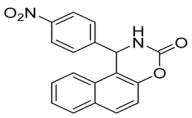 | 89 | 188 |
| 3 | 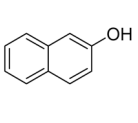 | 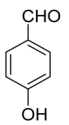 | 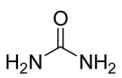 | 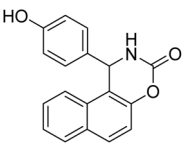 | 85 | 182 |
| 4 | 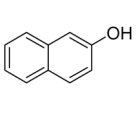 | 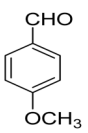 | 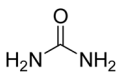 | 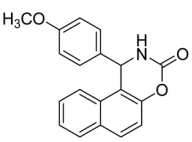 | 86 | 183 |
| 5 | 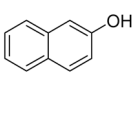 | 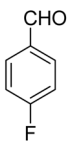 | 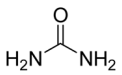 | 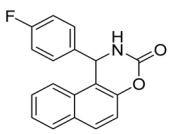 | 82 | 203 |
| 6 | 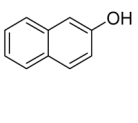 | 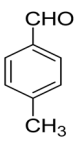 | 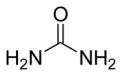 | 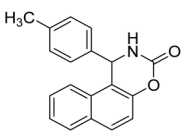 | 87 | 168 |
| 7 | 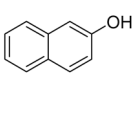 | 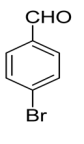 | 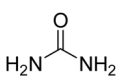 | 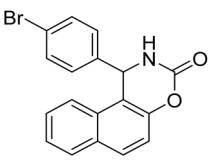 | 85 | 225 |
| 8 | 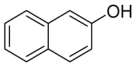 | 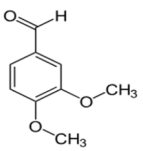 | 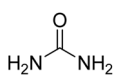 | 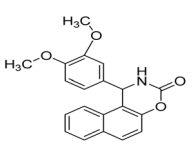 | Trace | |

[a] Reaction condition: aryl aldehyde (1 mmol), β-naphthol (1 mmol) and urea in presence of catalyst $Ni_{0.5}Zn_{0.5}Fe_2O_4$ (80 mg), at a temperature of 120 °C under solvent free condition.

carbonyl group. This facilitates the reaction of aryl aldehydes with beta-naphthol, generating an intermediate.[58] Again, the catalyst activates the intermediate and thus accelerates intramolecular cyclization to give the desired product. It was reported previously that the use of smaller catalyst particles (10 nm in the present work) can enhance the catalytic performance by reducing the diffusion path, providing more active sites, enhancing stability and workability under reactive environments.[59–61]

Semi-empirical calculations provide a reliable method for the study of organic reaction mechanisms, balancing computational efficiency in modelling chemical processes, structures and properties to give evidence for the proposed mechanism.[62] Theoretical calculations were performed to predict the transition state using the semiempirical PM6 method. The proposed mechanism is in agreement with the theoretically obtained transition state. The transition state obtained and IRC pathway details are included in the ESI.†

After optimizing the reaction conditions, in order to study the electronic effect of substituted aryl aldehydes, the reactions have been repeated with a variety of substituted aryl aldehydes with electron releasing and electron withdrawing groups while keeping 1 and 3 as fixed substrates. The results are summarized in Table 5. The yield of the product depends on both the electronic effect of reactants and the polarity of the carbonyl group in aldehydes. Aromatic aldehydes with both electron-donating and electron-withdrawing groups reacted and gave the products in good yields. Aldehydes with electron withdrawing groups gave higher yields (Table 5). Poor yield of product was obtained when using veratraldehyde, which may be due to the steric hindrance.

### 3.3 Recyclability studies

Recyclability is crucial in terms of economy and sustainability. The catalytic process was repeated over three consecutive reaction cycles to study the recyclability of the catalyst. Magnetic separation is an important property for the separation and reuse of nano-catalysts. The super paramagnetic nature of the NZF nanocatalyst enables the separation of the catalyst from the reaction mixture using a permanent magnet by magnetic recovery. The separation of magnetic solid catalysts was found to be fast, simple, convenient, and efficient by using an external magnet. After each cycle, the catalyst has been washed with ethanol at 60 °C, dried and used again. It was found out that the NZF catalyst can be reused three times without any significant loss of catalytic activity towards the synthesis of 1,2-dihydro-1-arylnaphtho[1,2-*e*] [1,3] oxazine-3-ones. The variation of percentage yield with the number of cycles is depicted as Fig. 4.

The $H^1$-NMR and $C^{13}$-NMR spectral data of the products are incorporated in the ESI file.†

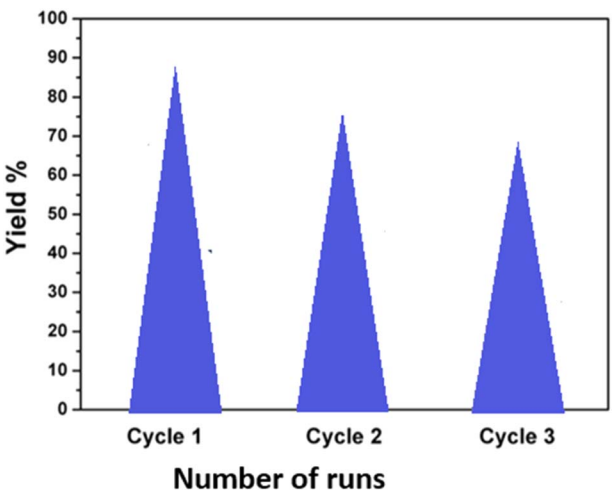


Fig. 4 Recyclability of the catalyst.

## 4 Conclusions

The work presented here demonstrated a novel approach to the synthesis of 1,2-dihydro-1-aryl naphtho [1,2-*e*] [1,3] oxazine-3-ones using the nanocatalyst $Ni_{0.5}Zn_{0.5}Fe_2O_4$. The NZF nanocatalyst was prepared by using a sol–gel auto combustion method, involving the reaction between Fe $(NO_3)_3 \cdot 9H_2O$, Ni $(NO_3)_2 \cdot 6H_2O$ and Zn $(NO_3)_2 \cdot 6H_2O$. The prepared NZF catalysts were found to be magnetically separable and demonstrated promising catalytic efficiency for organic conversions. The catalyst proved to be an effective heterogeneous catalyst for the one-pot synthesis of naphthoxazinones, which are of significant medicinal importance. The reaction involved three-component coupling of β-naphthol, aromatic aldehydes and urea using the NZF nanocatalyst, which had several advantages like high yield, environmental suitability and simple work-up procedure. A mechanism was proposed for the reaction, which was further supported by computational studies. The catalyst was recovered and reused without significant loss in the catalytic activity. The structures of the newly synthesized products were confirmed through spectroscopic data. The study demonstrated that the NZF nanocatalyst provided a promising route for the synthesis of naphthoxazinones and similar compounds in organic synthesis.

## Data availability

Data will be made available on request.

## Author contributions

Sreelakshmi Sreekandan: data curation, formal analysis, investigation, validation, methodology, writing – original draft; Anjitha Thadathil: data curation; Bindu Mavila: data curation; Kannan Vellayan: conceptualization, project administration, supervision, writing – review and editing; Pradeepan Periyat: conceptualization, supervision, writing – review and editing.

## Conflicts of interest

The authors declare no conflicts of interest.

## Acknowledgements

The authors are grateful to Government College for Women, Thiruvananthapuram, for NMR analysis.

## References

1 K. Hemalatha, G. Madhumitha, A. Kajbafvala, N. Anupama, R. Sompalle and S. M. Roopan, *J. Nanomater.*, 2013, **2013**, 4.
2 S. Khaturia, M. Chander, H. Sachdeva, Sangeeta and C. B. Mahto, *J. Nanomed. Nanotechnol.*, 2020, **11**, 1.
3 S. G. Babu and R. Karvembu, *Catal. Surv. Asia*, 2013, **17**, 156.
4 M. B. Gawande, A. K. Rathi, P. S. Branco and R. S. Varma, *Appl. Sci.*, 2013, **3**, 656.
5 P. Singh, S. Misra, A. Sahoo and S. Patra, *Sci. Rep.*, 2011, **11**, 9305.
6 J. A Mata, F. E Hahn and E. Peris, *Chem. Sci.*, 2014, **5**, 1723.
7 H. Lv, A. Lopes, d. Xu and B. Liu, *ACS Cent. Sci.*, 2018, **4**, 1412.
8 S. Cai, D. Wang, Z. Niu and Y. Li, *Chin. J. Catal.*, 2013, **34**, 1964.
9 L. Qina, Z. Zengb, G. Zenga, C. Laia, A. Duana, R. Xiaob and D. Huanga, *Appl. Catal.*, 2019, **259**, 1180.
10 X. Jia, J. Wang and E. Wang, *Adv. Mater.*, 2024, **36**, 2309261.
11 M. Sajjadi, S. Iravani, R. S. Varma and N. M. Nasrollahzadeh, *Nanomaterials*, 2020, **10**, 1784.
12 N. Maji and H. S. Dosanjh, *Magnetochemistry*, 2023, **9**, 156.
13 M. Amiri, K. Eskandari and M. S. Niasari, *Adv. Colloid Interface Sci.*, 2019, **271**, 101982.
14 W. Huang, S. Pan, Q. Yu, X. Liu, Y. Liu and R. Liu, *J. Inorg. Organomet. Polym. Mater.*, 2019, **29**, 1755.
15 E. Leal, S. T. Basílio, J. Dantas, P. Richa, R. da C. Lima, R. H. G. A. Kiminami and A. C. F. de M. Costa, *Arabian J. Chem.*, 2020, **13**, 8100.
16 S. S. Hossain and P. K. Roy, *J. Mater. Sci.:Mater. Electron.*, 2017, **28**, 18136.
17 S. T. Fardood, A. Ramazani, Z. Golfar and S. W. Joo, *Appl. Organomet. Chem.*, 2017, **31**, 3823.
18 P. Saha, S. Das and S. Sutradhar, *J. Appl. Phys.*, 2018, **124**, 045303.
19 M. A. Dar, V. Verma, S. P. Gairola, W. A. Siddiqui, R. K. Singh and R. K. Kotnala, *Appl. Surf. Sci.*, 2012, **258**, 5342.
20 J. Dantas, J. R. D. Santos, R. B. L. Cunha, R. H. G. A. Kiminami and A. C. F. M. Costa, *Mater. Res.*, 2013, **16**, 625.
21 L. Ma, L. Chen and S. Chen, *Mater. Chem. Phys.*, 2009, **114**, 692.
22 S. B. Madake, J. B. Thorat and K. Y. Rajpure, *Sens. Actuators, A*, 2021, **331**, 112919.
23 B. I. Kharisov, H. V. R. Dias and O. V. Kharissova, *Arabian J. Chem.*, 2019, **12**, 1234.
24 S. B. Singh and P. K. Tandon, *J. Energy Chem.*, 2014, **2**, 106.
25 B. P. Rickard, M. Overchuk, G. Obaid, M. K. Ruhi, U. Demirci, S. E. Fenton, J. H. Santos, D. Kessel and I. Rizvi, *J. Photochem. Photobiol., A*, 2023, **99**, 448.
26 S. T. Fardood, F. Moradnia, S. Heidarzadeh and A. Naghipour, *Nanochem. Res.*, 2023, **8**, 134.
27 F. Alantari, S. Rezayati, A. Ramazani and M. R. Poor Heravi, *Appl. Organomet. Chem.*, 2023, **37**, e7064.
28 S. T. Fardood, F. Moradnia and T. M. Aminabhavi, *Environ. Pollut.*, 2024, **358**, 124534.
29 L. M. Nainwal, S. Tasneem, W. Akhtar, G. Verma, M. F. Khan, S. Parvez, M. Shaquiquzzaman, M. Akhter and M. M. Alam, *Eur. J. Med. Chem.*, 2019, **164**, 121.
30 X. Xu, Z. Guo, D. Zhu, J. Pan, C. Yang and S. Li, *Process Saf. Environ. Prot.*, 2024, **183**, 59.
31 A. Hajra, D. Kundu and A. Majee, *J. Heterocycl. Chem.*, 2009, **46**, 1019.
32 E. Kabir and M. Uzzaman, *Results Chem.*, 2022, **4**, 100606.
33 E. Vitaku, D. T. Smith and J. T. Njardarson, *J. Med. Chem.*, 2014, **57**, 10257.
34 A. Chanderiya, R. Das, G. Naikoo, I. U. Hassan, S. K. Kashaw and S. Pandey, *Chem.–Asian J.*, 2021, **33**, 949.
35 S. Rezayati, M. M. Moghadam, Z. Naserifar and A. Ramazani, *Inorg. Chem.*, 2024, **63**, 1652.
36 M. Kumar, A. K. Singh, V. K. Singh, R. K. Yadav, A. P. Singh and S. Singh, *Coord. Chem. Rev.*, 2024, **505**, 215635.
37 W. Su, W. Tang and J. Li, *J. Chem. Res.*, 2008, **3**, 123.
38 A. Chaskar, V. Vyavhare1, V. Padalkar1, K. Phatangare and H. Deokar, *J. Serb. Chem. Soc.*, 2011, **76**, 21.
39 J. X. Ji, L. Q. Qiu, C. W. Yip and A. S. C. Chan, *J. Org. Chem.*, 2003, **68**, 1589.
40 A. S. Dzunuzovic, N. I. Ilic, M. V Petrovic, J. D. Bobic, B. Stojadinovic, M. Z. Dohcevic and B. D. Stojanovic, *J. Magn. Magn. Mater.*, 2015, **374**, 245.
41 S. T. Fardood, A. Ramazani, M. Ayubi, M. F Moradnia, S. Abdpoura and R. Forootana, *Chem. Methodol.*, 2019, **3**, 519.
42 M. Lei, L. Ma and L. Hu1, *Tetrahedron Lett.*, 2009, **50**, 6393.
43 J. H. Forsberg, V. T. Spaziano, T. M. Balasubramanian, G. K. Liu, S. A. Kinsley, C. A. Duckworth, J. J. Poteruca, P. S. Brown and J. L. Miller, *J. Org. Chem.*, 1987, **52**, 1017.
44 O. Yavuz, M. K. Ram, M. Aldissi, P. Poddar and S. Hariharan, *J. Mater. Chem.*, 2005, **15**, 810.
45 A. Rostamnejadi, H. Salamati and P. Kameli, *J. Supercond. Novel Magn.*, 2012, **25**, 1123.
46 K. Praveena and K. Sadhana, *Int. J. Sci. Res. Publ.*, 2015, **5**, 1.
47 A. B. Mapossa, J. Dantas, M. R. Silva, R. H. Kiminami, A. C. F. Costa and M. O. Daramola, *Arabian J. Chem.*, 2020, **13**, 4462.
48 R. Thejas, T. L. Saundariya, G. Nagaraju, K. Swaroop, S. C. Prashantha, M. Veena, E. Melagiriyappa and C. S. Naveen, *Mater. Lett.:X*, 2022, **15**, 10015.
49 C. S. M. Havan, M. K Babrekar, S. S. More and K. M. Jadhav, *J. Alloys Compd.*, 2010, **507**, 21.
50 J. Massoudi, M. Smari, K. Nouri, E. Dhahri, K. Khirouni, S. Bertaina, L. Bessais and E. K. Hill, *RSC Adv.*, 2020, **10**, 34556.
51 S. Toh, C. B. Mcauly, K. Tschulik, M. Uhlemann, A. Crossley and R. C. Compton, *Nanoscale*, 2013, **5**, 4884.
52 R. Sharmal, D. P. Bisen, U. Shukla and B. G. Sharma, *Recent Res. Sci. Technol.*, 2012, **4**, 77.
53 A. Kocjan, M. Logar and Z. Shen, *Sci. Rep.*, 2017, **7**, 2541.

54 H. Yin, P. S. Casey, M. J. McCall and M. Fenech, *Langmuir*, 2010, **26**, 15399.
55 R. K. Singh, R. Bala and S. Kumar, *Indian J. Chem.*, 2016, **55**, 381.
56 H. Moghanian, A. Mobinikhaledi, A. G. Blackman and E. S. Farahani, *RSC Adv.*, 2014, **5**, 2816.
57 J. W. M. Crawley, I. E. Gow, N. Lawes, I. Kowalec, L. Kabalan, C. R. A. Catlow, A. J Logsdail, S. H Taylor, N. F. Dummer and G. J. Hutchings, *Chem. Rev.*, 2022, **122**, 6795.
58 A. R. Liandi, A. H. Cahyana, A. J. F. Kusumah, A. Lupitasari, D. N. Alfariza, R. Nuraini, R. W. Sari and F. C. Kusumasari, *Case Stud. Chem. Environ. Eng.*, 2023, **7**, 100303.
59 P. Li and H. C. Zeng, *ACS Appl. Mater. Interfaces*, 2016, **8**, 29551.
60 S. Chaturvedi, P. N. Dave and N. K. Shah, *J. Saudi Chem. Soc.*, 2012, **16**, 307.
61 A. Chaudhary, *Mol. Diversity*, 2021, **25**, 1211.
62 F. Passamani, I. A. Guerra, P. R. Filgueiras, B. A. M. C. Santos and A. de Silva Goncalves, *Orbital:Electron. J. Chem.*, 2022, **14**, 168.